The Coordination Chemistry of Oxide and Nanocarbon Materials

ARTICLE

The Coordination Chemistry of Oxide and Nanocarbon Materials

Elena Bekyarova* and Matthew P. Conley*

Understanding how a ligand affects the steric and electronic properties of a metal is the cornerstone of the inorganic chemistry enterprise. What happens when the ligand is an extended surface? This question is central to the design and implementation of state-of-the-art functional materials containing transition metals. This perspective will describe how these two very different sets of extended surfaces can form well-defined coordination complexes with metals. In the Green formalism, functionalities on oxide surfaces react with inorganics to form species that contain X-type or LX-type interactions between the metal and the oxide. Carbon surfaces are neutral L-type ligands; this perspective focuses on carbons that donate six electrons to a metal. The nature of this interaction depends on the curvature, and thereby orbital overlap, between the metal and the extended π-system from the nanocarbon.

Introduction

Reactions of inorganic small molecules with extended surfaces have potential far reaching implications at the forefront of materials science. Two examples close to the authors of this perspective are catalytic reactions with heterogeneous catalysts and nano-electrical engineering of carbon materials. Many large-scale chemical feedstocks are products of reactions involving heterogeneous catalysts, usually an inorganic or organometallic active site formed under reaction conditions supported on a high surface area oxide.[1] Carbon nanostructures are broadly applicable in printable electronics, opto-electronics, energy conversion/storage, and catalysis; chemical functionalization of these materials in a rational and predictive manner is a long-term goal to engineer the properties of these materials for these applications.[2-8] These two examples from seemingly disparate fields within materials science require some degree of orthogonal chemical modification of a surface with small molecule inorganics or organometallics to approach long-standing challenges where chemical structure predicts physical properties.

This perspective will describe selected examples showing how surfaces affect the coordination chemistry of transition metal complexes with a primary focus on how basic chemical insights can predict which species are most likely to form on a given surface. We will focus on oxide surfaces and a selection of nanocarbon materials. The former are broadly important in heterogeneous catalysis, while the latter have applications in electrocatalysis[9] and nanoelectronics.[10] As will be discussed below, the design principles to form well-defined inorganic or organometallic structures on these types of materials vary because of the fundamental differences in the interactions between a metal and the functional groups on an oxide or nanocarbon surface.

A Reductionist Approach to Coordination Chemistry on Oxide or Carbon Surfaces

The inorganic chemistry community has a long history of parameterizing properties of ligands to simplify predictive outcomes in chemical reactions. Figure 1 shows the classic example of R_3P–$Ni(CO)_3$ used by Tolman to optimize the reactivity and selectivity in the hydrocyanation of butadiene.[11] The two critical parameters that emerged from these studies were the cone angle (θ), which describes the steric properties of the phosphine, and the ν_{CO} stretch, which describes the donor ability of the phosphine. Though the more generally applicable buried volume is gradually replacing θ as a steric parameter,[12] these parameters continue to permeate the community interested in optimization of ligand properties.
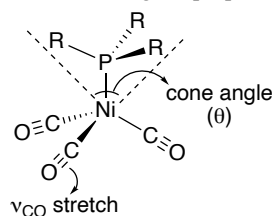

Figure 1. Tolman parameters used in $R_3PNi(CO)_3$.

Surfaces are notoriously complex, but similar reductionist approaches have merit when considering how metals will interact with the various sites present on a surface. For example, with few exceptions,[13] nearly all reactions involving an oxide and an organometallic involves protonolysis of a reactive L_nM–X (X = alkyl, amido, alkoxide, halide etc.) by a hydroxyl group (–OH), eq 1.[14-21] The products of this reaction will chiefly depend on the acidity of the –OH group present on the oxide surface.[22] The silanols present on silica are relatively weak Brønsted acids and tend to form the covalent species shown in eq 1. Oxides that contain –OH groups that are stronger Brønsted acids tend to form the ion-pairs shown in eq 1. Though this simplification is very useful, there are several caveats that must also be considered when predicting structure on oxides. As will be discussed in some detail below even applying the assumption that acidity of surface –OH groups affects the speciation as shown in eq 1 requires considerable care.

a. *Department of Chemistry, University of California, Riverside, California 92521, United States*
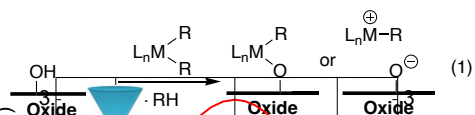
Carbon surfaces require an entirely different reductionist approach. A transition metal has the highest probability of interacting with the extended π-surface on a carbon nanomaterial.[10, 23, 24] The symmetries of the orbitals that describe the extended π-surface of graphene are shown in Figure 2a and are isolobal to the e_{2u} LUMO of benzene and the e_{1g} HOMO of benzene, but these orbitals are degenerate (i.e. the HOMO-LUMO gap is 0 eV) at the Dirac point of graphene.[25-28] Therefore, graphene surfaces are expected to react with transition metals to form surface species that are similar to molecular η6-arene complexes.
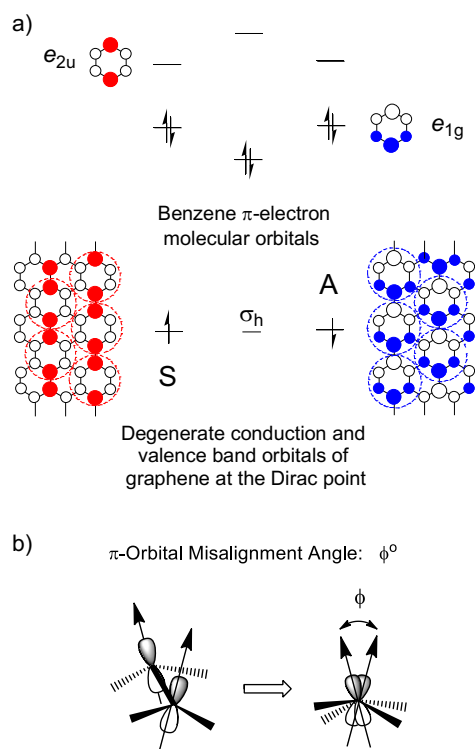

Figure 2. The e_{2u} LUMO and e_{1g} HOMO orbitals of benzene are shown together with the orbitals for graphene at the Dirac point (a). Reprinted with permission from ref 10. Copyright 2013 American Chemical Society. The π-orbital misalignment angle (φ) encountered in the FMOs of carbon nanotubes (b).

The orbital scheme shown in Figure 2a for graphene also applies to carbon nanotubes, but curvature from the nanotube induces misalignment of the π-FMOs shown in Figure 2b. As the diameter of the nanotube decreases the π-orbital misalignment increases. For example, φ is 18.5° for a (10,0) SWCNT with a diameter of 7.81 Å, and φ increases to 21.3° for a (5,5) SWCNT with a diameter of 6.76 Å.[29, 30] The curvature-induced misalignment of the π-orbitals of the carbon atoms affects the overlap of the SWCNT π-FMOs with substrates in functionalization reactions, and contrasts SWCNTs with graphene.

The remainder of this perspective will describe how these reductionist models for these two very different surfaces result in well-defined materials. The reader will notice that there is significantly more emphasis placed on the formation of well-defined

sites on oxides. One reason for this emphasis is related to the long history of the surface organometallic community contributing to the characterization sites on surfaces using analytical methods familiar to the small molecule inorganic chemist. Another reason is that there are simply fewer examples of metals coordinating to carbon surfaces to form well-defined coordination complexes, with exception given to functionalization of oxidized graphitic carbons[9, 31-33] that do not interact with the metal through the extended π-surface of the nanocarbon.

The Coordination Chemistry of Silica Dehydroxylated at 700 °C: The Most Common Support for Surface Organometallic Chemistry

The "model" surface illustrating some of the reaction trends in eq 1 is Aerosil-200 (200 m²/g), a non-microporous hydrophilic silica. When this material is dehydroxylated at 700 °C (SiO_{2-700}) a low coverage of ~0.8 ≡Si–OH nm⁻² is present on the silica surface.[34] Most of the silanols on the partially dehydroxylated surface are isolated silanol groups. In the Green formalism,[35] silanols on silica surfaces can act as either a X-type ligands to form ≡Si–O–M, or LX-type ligands that coordinate nearby siloxane bridges in addition to ≡Si–O–M. Silica surfaces are amorphous, prohibiting advanced X-ray diffraction studies of native or functionalized silica surfaces that are common in crystalline extended solids,[36] though recent advances in solid-state NMR and computational methods provide three-dimensional structures of sites present on oxide surfaces.[37-39] In the absence of extensive characterization to determine LX-type ligand coordination for silica-supported organometallics the X-type ligand behavior of silanols on silica is assumed. Using X-ray absorption methods κ^2-≡SiO–Ta(=CHᵗBu)(CH₂ᵗBu)₂(≡Si–O–Si≡),[40] κ^2-≡SiO–W(=NAr)(=CHᵗBu)(CH₂ᵗBu)(≡Si–O–Si≡),[41] κ^2-≡SiO–Re(=CHᵗBu)(≡CᵗBu)(CH₂ᵗBu)(≡Si–O–Si≡),[42] κ^2-≡SiO–W(=O)(CH₂ᵗBu)₃(≡Si–O–Si≡),[43] and κ^2-≡SiO–Lu[CH(SiMe₃)₂]₂(≡Si–O–Si≡)[44] were shown to coordinate a nearby ≡Si–O–Si≡ bridge, Figure 3. These structures have variable sterics and electronics at the metal, suggesting that LX-type ligand coordination is quite common.
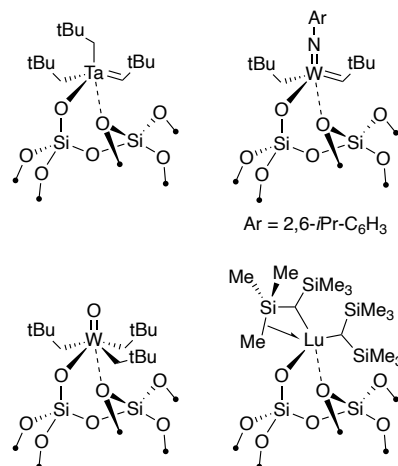
Figure 3. Examples of silica behaving as an LX-type ligand.

Solid-state NMR trends can also imply the presence or absence of a coordinated ≡Si–O–Si≡ bridge. The ¹³C cross polarization magic angle spinning (CPMAS) NMR spectrum of ≡SiO–TaMe₂Cl₂[45] or ≡SiO–TiMe₃[46] contain two signals for Ta–Me or Ti–Me, respectively, consistent with the presence of both κ^1- and κ^2- isomers on the silica surface. This data also suggests that the two isomers exchange slowly on the NMR timescale. Direct observation of a coordinated ≡Si–O–

Si≡ bridge is also possible using ^{17}O MAS NMR spectroscopy of functionalized [17]O enriched silica.[47]

Scandium has one NMR active nucleus ([45]Sc, $I = 7/2$, $\gamma = 6.5081$ x 10^7 rad T[-1] s^{-1},100 % abundant), and the lineshape of the [45]Sc NMR signal is very sensitive to structure.[48,49] Cp*$_2$Sc–Me (Cp* = pentamethylcyclopentadienyl) reacts with SiO$_{2-700}$ that forms a mixture of κ^1-Cp*$_2$Sc–OSi≡ and κ^2-Cp*$_2$Sc(OSi≡)(≡Si–O–Si≡), Figure 4a.[50] The static [45]Sc NMR spectrum of κ^1-Cp*$_2$Sc–OS≡ and κ^2-Cp*$_2$Sc(OSi≡)(≡Si–O–Si≡) shown in Figure 4b was simulated as two scandium sites with quadupolar coupling constants (C$_Q$) of 35.4 and 21.9 MHz, respectively. Trends in C$_Q$ for Cp*$_2$Sc–R,[51] Cp*$_2$Sc–X,[52] and Cp*$_2$ScX(THF)[52] shown in Figure 4c; experimental [45]Sc NMR data for Cp*$_2$Sc–OR (R = CMe$_2$CF$_3$, CMe(CF$_3$)$_2$, C(CF$_3$)$_3$, SiPh$_3$); and DFT modeling support these assignments. Similar surface heterogeneities were also resolved in ^{27}Al NMR studies of Al[N(SiMe$_3$)$_3$]$_2$Cl(THF) supported on silica.[53]

Cp*$_2$ScX(THF) (c) and. Figures reproduced with permission from ref 50 (b, c).

The LX-type ligand behavior affects the structure and properties of the metal. For example, the lanthanides in Ln[CH(SiMe$_3$)$_2$]$_3$ (Ln = Y,[54] La,[55] Ce,[54] Sm,[55] Lu[44]) interact with the three proximal Si–Me groups to form bridging 3c-2e μ-Me structures. XAS studies of κ^2-≡SiO–Lu[CH(SiMe$_3$)$_2$]$_2$(≡Si–O–Si≡) show that only one proximal Si–Me interacts with lutetium, suggesting that coordination of a siloxane bridge prevents weak secondary interaction in lanthanides. This is consistent with solid-state NMR studies of ≡SiO–Y[N('Bu)(SiHMe$_2$)]$_2$[56] and ≡SiO–La[CH(SiHMe)$_3$]$_3$[57, 58] that contain weaker more fluxional Ln•••H–Si secondary interactions than their respective homoleptic compounds in solution. The Lu•••Me–Si distance in κ^2-≡SiO–Lu[CH(SiMe$_3$)$_2$]$_2$(≡Si–O–Si≡) is 2.80(2) Å, shorter than the three Lu•••Me–Si distances in Lu[CH(SiMe$_3$)$_2$]$_2$ (2.973(3) Å). This result suggests that the lutetium organometallic is more Lewis acidic when supported on silica, certainly due in part to the replacement of one Lu–C bond by a Lu–O bond.

LX-coordination of silica to metals also affects reactivity. Opening ≡Si–O–Si≡ bridges occurs in reactions of silica-supported organometallics when treated with H$_2$ to form metal hydrides.[17, 59, 60] These reactions are undeniably complex, but probably occur through κ^2-coordination of the metal hydride intermediates to the silica surface, as shown in Figure 5 for the reaction of ≡Si–O–Zr(CH$_2$'Bu)$_3$ with H$_2$ to from (≡Si–O)$_3$ZrH and (≡Si–O)$_2$ZrH$_2$.[61, 62] Indeed, this reactivity trend is quite common. Opening siloxane bridges are also involved in thermolysis of organometallics supported on silica,[63-65] and in reactions of organoaluminum,[66-73] organogallium,[74-76] or organotin[77] compounds with silica. Less clear is if this reactivity is also important in the generation of Zr–H species on silica-alumina materials, which are active in polyethylene polymerization and C–C hydrogenolysis reactions,[78] and can be generated in the presence of triisobutylaluminum activators.[79]
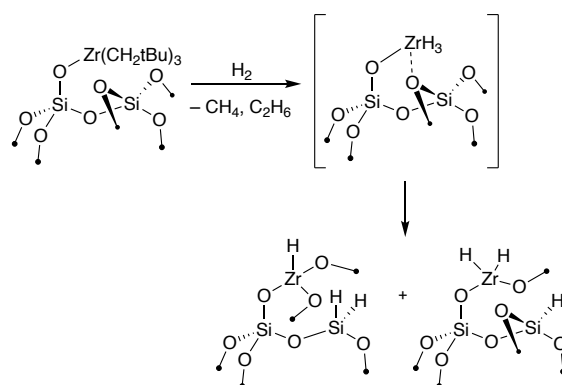
Figure 5. Hydrogenolysis of Zr–R bonds on silica result in hydride transfer to the surface through siloxane bridge opening.

Silica supported metal alkylidenes for olefin metathesis are some of the most extensively studied well-defined heterogeneous catalysts.[80] These studies show the effects of a siloxy ligand on the catalytic behavior of the supported metal alkylidene. For example, κ^2-≡SiO–Re(=CH'Bu)(≡C'Bu)(CH$_2$'Bu)(≡Si–O–Si≡) is significantly more reactive in olefin metathesis than Re(=CH'Bu)(≡C'Bu)(CH$_2$'Bu)$_2$.[81] This is due to the dissymmetric electronic ligand environment at Re that reduces the barrier to olefin coordination and 2+2 cycloaddition,[82] a key design strategy in state-of-the-art homogeneous catalysts for Z-selective olefin metathesis.[83-85] In addition to the electronic effects, the siloxy ligand on silica is sterically small. For example, the very bulky

Figure 4. Reaction of Cp*$_2$Sc–Me with SiO$_{2-700}$ (a); static [45]Sc{^{1}H} NMR spectrum of κ^1-Cp*$_2$Sc–OSi≡ (large C$_Q$) and κ^2-Cp*$_2$Sc(OSi≡)(≡Si–O–Si≡) (small C$_Q$) showing simulations for both sites (red), experimental spectrum (black), and individual site simulations (blue and green, b); C$_Q$ for Cp*$_2$Sc–R, Cp*$_2$Sc–X, and

(AdPO)$_2$W(=CH^{t}Bu)(=O) (AdPO = 2,6-diadamantylphenoxide) reacts to form (AdPO)$_2$W(=O)(trans-4,4-dimethyl-2-ene) and is unreactive in olefin metathesis.[86] However, (AdPO)$_2$W(=CH^{t}Bu)(=O) reacts with SiO$_{2-700}$ to form ≡SiO–W(=CH^{t}Bu)(=O)(AdPO), a more sterically open alkylidene that reacts with ethylene to form the square pyramidyl ≡SiO–W(CH$_2$)$_3$(=O)(AdPO) and is a very active and stable supported metathesis catalyst (Figure 6a).[87]

Olefin metathesis catalysts supported on silica are often more stable than homogeneous analogues due to site-isolation of active site that prevents bimolecular decomposition, common in sterically open homogeneous catalysts.[88-90] Site-isolation broadly effects the behavior of supported organometallics, such as the generation of coordinatively unsaturated metal hydrides discussed above.[59] A more recent example that illustrates this point is the reaction of (^{t}BuCH$_2$)$_3$Ta=Ir(H)$_2$Cp* with silica followed by H$_2$ treatment to form ≡SiO–Ta(CH$_2$^{t}Bu)(H)(=Ir(H)$_2$Cp*), Figure 6b.[91] In solution (^{t}BuCH$_2$)$_3$Ta=Ir(H)$_2$Cp* reacts with H$_2$ to form tetranuclear clusters that are unable to form on silica surfaces due to site-isolation.
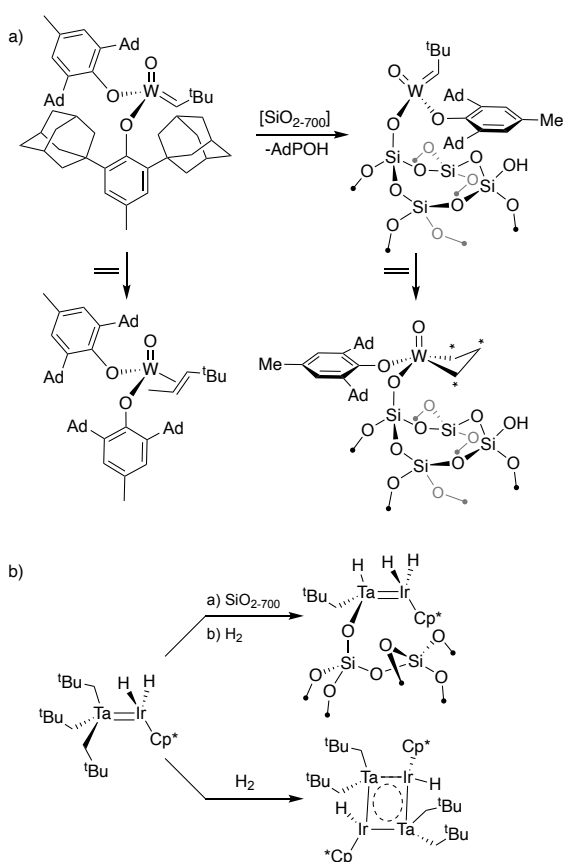

Figure 6. Effects of a siloxy ligand from silica on the reactivity of a W-oxo alkylidene (a) and the reactivity of (^{t}BuCH$_2$)$_3$Ta=Ir(H)$_2$Cp* in the presence of H$_2$ in solution or supported on silica (b).

Generation of Ion-pairs on Surfaces

Organometallic ion-pairs play an important role in catalysis.[92] In a systematic study of the reaction of Cp*IrMe$_2$(PMe$_3$) with partially dehydroxylated oxides to form Cp*IrMe(PMe$_3$)(oxide) or [Cp*IrMe(PMe$_3$)][oxide. Only oxides capable of forming ion-pairs, such as sulfated zirconium oxide (**SZO**), resulted active catalysts for H/D exchange reactions.[93] This is due to reversible coordination of the Ir fragment to the weakly coordinating surface sites on present on

SZO that under reaction conditions form [Cp*Ir(C$_6$D$_5$)(PMe$_3$)]$^+$ capable of activating C-H bonds in substrates, Figure 7.
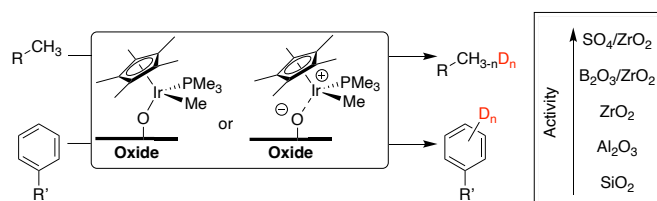

Figure 7. H/D exchange of arenes and alkanes catalyzed by supported Cp*IrMe(PMe$_3$) on oxides doped with different anions.

The reason **SZO** forms ion-pairs and silica does not from ion-pairs with organometallics is related to the acidity of –OH groups on these surfaces. As the strength of a Brønsted acid (HX) increases the anionic conjugate base (X$^-$) forms weaker ion-pairs.[94-96] Experimental correlations between solid acid strength and solution acid strength are difficult to obtain,[97-100] but DFT methods are fairly accurate at reproducing experimental deprotonation energies (DPE) of Brønsted acids in the gas phase. For example, the most stable structures of the acidic sites present on **SZO** were modeled on periodic (101) or (001) ZrO$_2$ surfaces as tripodal sulfate sites with protons dissociated from the sulfate lying on nearby Zr–O–Zr bridges (Figure 8a).[101] The calculated deprotonation energies of these Brønsted acid sites range from 320 – 370 kcal mol^{-1}, significantly higher than the gas phase acidity of H$_2$SO$_4$ (302.3 kcal mol^{-1}),[102] but more acidic than simple small molecule silanols (359.3 kcal mol^{-1}).[103]
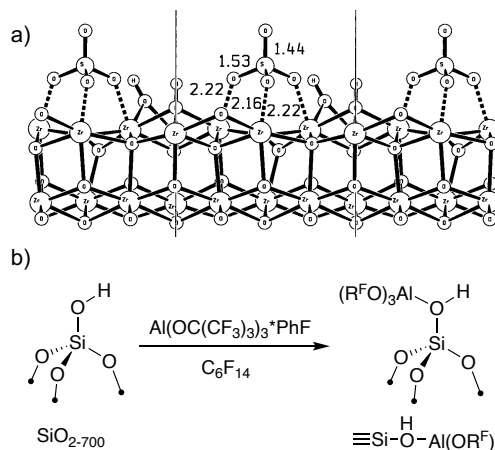
Figure 8. Equilibrium structure of the (101) surface of ZrO$_2$ after H$_2$SO$_4$ adsorption (a); reaction of SiO$_{2-700}$ with Al(OC(CF$_3$)$_3$)$_3$(PhF) to form ≡Si–OH–Al(OR^F)$_3$. Figure 8a reproduced with permission from Ref 101.

Surfaces more weakly coordinating than the sulfates on **SZO** should contain very strong Brønsted acid –OH group. Brønsted superacidity is common in mixtures of Lewis acids and Brønsted acids,[104, 105] and these mixtures contain mixtures of weakly coordinating anions. Therefore, contacting the fairly weak Brønsted acid ≡Si–OH groups on SiO$_{2-700}$ with a very strong Lewis acid should "activate" silica to form weakly coordinating ion-pairs. The reaction of Al(OC(CF$_3$)$_3$)$_3$(PhF)[106] with SiO$_{2-700}$ forms the well-defined bridging silanols ≡Si–OH–Al(OR^F)$_3$ (Figure 8b, R^F = C(CF$_3$)$_3$).[107] DFT calculations of small clusters that approximate the structure of the bridging silanols, which match key spectroscopic signatures obtained experimentally, give a DPE of 267.2 kcal mol^{-1}. This value indicates that ≡Si–OH–Al(OR^F)$_3$ is significantly more acidic than

triflic acid (expt DPE = 299.5 kcal mol⁻¹) but less acidic that state-of-the-art weakly coordinating carborane or aluminate anions (DPE of H[Al(OR^F)₄] = 248.8,[108] DPE of H[CHB₁₁Cl₁₁] = 239.1[94]).

The connection between ion-pairing and structure is perhaps clearest in studies of silylium (R_3Si^+) ions.[109-111] R_3Si^+ containing bulky alkyl groups and weakly coordinating carborane anions adopt planar structures expected for the sp² hybridized silicon,[112] but sterically open R_3Si^+ coordinate to weakly coordinating anions to form pyramidylized silylium-like ions, Figure 9.[113, 114] These structural features track with characteristic desheilded ²⁹Si NMR chemical shifts for "free" planar silylium ions that shift to lower chemical shift values for pyramidylized silylium-like ions. This behavior is related to the origin of the ²⁹Si NMR chemical shift.[109, 115] As silicon in R_3Si^+ becomes more pyramidylized the paramagnetic shielding (σ^p) decreases, resulting in progressively lower ²⁹Si NMR chemical shift values.
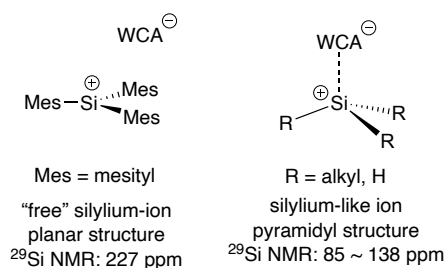

Figure 9. Structure and ²⁹Si NMR chemical shift of free Mes_3Si^+ and silylium-like ions.

SZO reacts with allyltriisopropylsilane to form [ⁱPr₃Si][**SZO**].[116] The solid-state ²⁹Si NMR spectrum of [ⁱPr₃Si][**SZO**] contains a major signal at 53 ppm, which is more deshielded that ⁱPr₃SiOTf (²⁹Si NMR = 41 ppm). ≡Si–OH–Al(OR^F)₃ also reacts with allyltriisopropylsilane

to form [ⁱPr₃Si][R^FO₃Al–OSi≡], and contains a ²⁹Si CPMAS NMR chemical shift at 70 ppm. These values are at significantly higher than the ²⁹Si NMR chemical shift in ≡Si–O–SiR₃ (²⁹Si NMR = 14 ppm),[117-119] and are consistent with the presence of silylium-like fragments in these materials. Indeed, [ⁱPr₃Si][**SZO**] activates sp³ C–F bonds in the presence of excess HSiEt₃ to give hydrocarbon products, and is more stable and reactive in hydrodefluorination reactions than high surface area AlCl₃₋ₓFₓ,[120] the only other heterogeneous catalyst for this reaction. However, R_3Si^+ ions containing weakly coordinating borate or carborane anions are more active and stable than either of these well-defined materials.[121, 122]

Figure 10 shows the relationship between Brønsted acidity of HX, ion-pairing, and ²⁹Si NMR chemical shift for a selected family of R₃Si–X (X = anion or surface site). The gas phase DPE of HCl is 336.2 kcal mol⁻¹. Reed showed [HNOct₃][X] in CCl₄ form contact ion pairs, and that the ν_NH stretch of the ammonium cation is a good measure of ion pairing.[94] The ν_NH of [HNOct₃][Cl] is 2330 cm⁻¹. The ²⁹Si NMR chemical shift of ⁱPr₃SiCl is 36 ppm. These data show that HCl is the weakest Brønsted acid, forms the strongest ion-pairs, and has the most shielded ²⁹Si NMR chemical shift shown in Figure 10. Increasing the Brønsted acidity results in blue-shifted ν_NH [HNOct₃][X] in CCl₄ solution, consistent with weaker ion-pair formation, and deshielded ²⁹Si NMR chemical shifts in [R₃Si][X].

These trends hold for the supported organosilanes shown in Figure 10. ≡Si–OH–Al(OR^F)₃ is the strongest heterogeneous Brønsted in Figure 10, when deprotonated forms weak ion pairs with [HNOct₃], and has the most desheilded ²⁹Si NMR chemical shift of the series. Decreasing Brønsted acidity, from DFT calculated DPE, results in lower field ²⁹Si NMR shifts of the supported organosilanes. This set of data indicates that ²⁹Si NMR chemical shift of supported organosilanes is a rapid method to assess if an oxide is likely to form ion pairs.
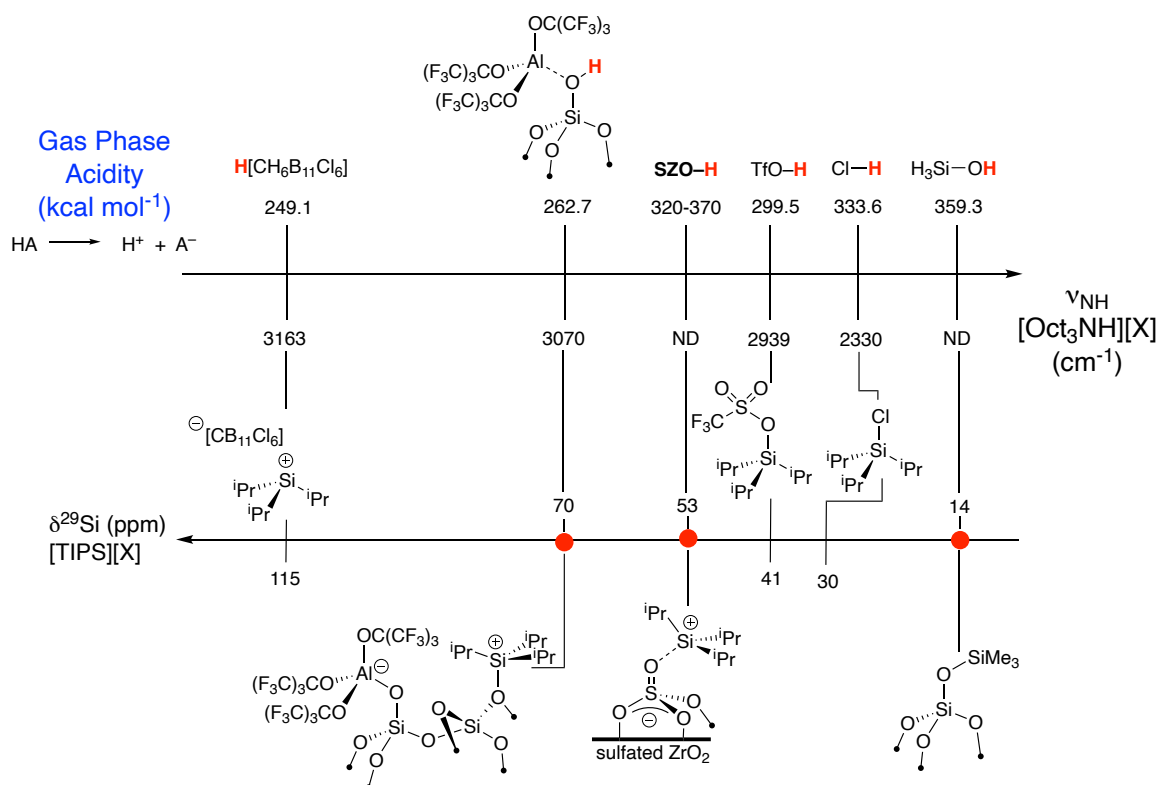
Figure 10. Relationship of gas phase acidity for HX, ν_{NH} for [Oct$_3$NH][X], and ^{29}Si NMR chemical shift of R$_3$Si–X.

Partially Dehydroxylated Al$_2$O$_3$ – A Limitation of the Reductionist Approach for Oxides?

The preceding discussion shows that acidity is useful to predict formation of reaction products shown in eq 1. Alumina shows interesting properties that break from this trend because the partially dehydroxylated alumina surface contains Lewis sites.[123, 124] Lewis sites on alumina bind N$_2$[125, 126] and activate unreactive C–H bonds,[127] indicating that they are very strong Lewis acids. Experimental characterization of the structure of these Lewis sites is elusive, but available data suggests either five-coordinate[128] or three-coordinate[129] aluminum sites are the origin of the strong Lewis acidity on aluminas.

Lewis sites on alumina are very important in catalysis, and more specifically in applications of partially dehydroxylated alumina as a support for well-defined organometallics. The studies showing this behavior generally relate to attempts to understand the heterogeneous Ziegler-Natta catalyst. The condensed timeline in Figure 11 shows key discoveries gradually building towards the understanding that M–R$^+$ (R = H, alkyl) catalyze this reaction in solution and on oxide supports. Ballard[130-132] and Yermakov[62, 133] studied reactions of homoleptic ZrR$_4$ complexes with alumina (Ballard)[130] or silica followed by treatment with H$_2$ to generate hydrides (Yermakov).[62] These initial studies were simultaneously disappointing and revealing. Both well-defined catalysts were significantly less active than traditional Ziegler-Natta compositions, but organozirconium species supported on alumina were more active than those supported on silica. The molecular origin of this activity difference was not characterized until studies by Marks showing that Cp*$_2$ThMe$_2$ reacts with highly dehydroxylated alumina to form organometallic ion pairs of [Cp*$_2$ThMe][MeAlO$_x$].[134] Similar behavior was also implicated in related organozirconium species supported on alumina.[135-141]
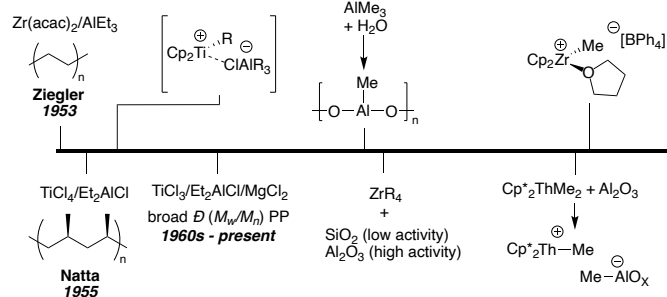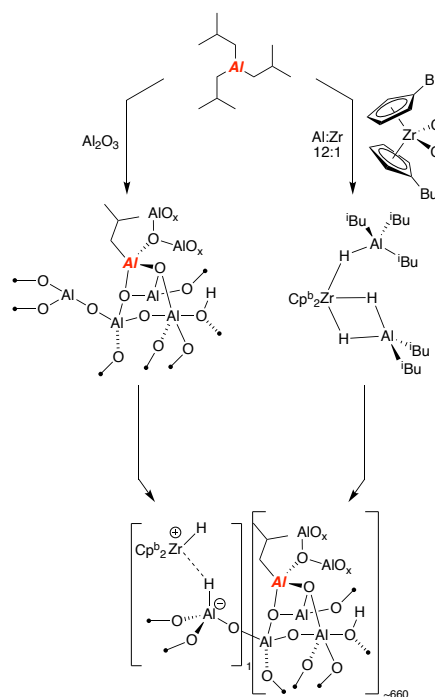

Figure 11. Evolution in the understanding of the Ziegler-Natta Catalyst for olefin polymerization, showing key discoveries for homogeneous (top) and heterogeneous (bottom) catalysts. Reproduced from ref 154.

The conclusions drawn from studies of the supported species parallel those found in solution. The first hints of electrophilic organometallics arose from studies of Cp$_2$TiCl$_2$ and Et$_2$AlCl by Breslow,[142] which are also related to intermediates formed in carboalumination reactions.[143] However, activated metallocenes were significantly less active than common heterogenous compositions until the serendipitous discovery of partially hydrolyzed AlMe$_3$ activators by Kaminsky and Sinn.[144] Isolation of Cp$_2$ZrMe(THF)$^+$ by Jordan established that cationic organometallics are important intermediates in this reaction,[145, 146] which was expanded upon by several other groups using various activators to access metalloceneium ions as weakly coordinated ion pairs.[147-151]

The insights obtained from studies from both the heterogeneous and homogeneous communities were critical to design industrial olefin polymerization catalysts that form *in-situ* from mixtures of a metallocene pre-catalyst, alkylaluminum, and alumina.[152, 153] The complexity of these mixtures is compounded by the series of steps and possible side reactions involved with alkylating a metallocene dichloride with alkylaluminum, reactions of alkylaluminum with Al–OH sites that could form surface activators similar to partially hydrolyzed AlMe$_3$, and/or unfavorable surface interactions between the metallocene and Al$_2$O$_3$.

Recently the role of each component in one of these mixtures containing Cp$^b_2$ZrCl$_2$ (Cp^b = 1-butylcyclopentadienyl), Al^{i}Bu$_3$, and Al$_2$O$_{3-600}$ was determined, Figure 12.[154] Typical mixtures containing 12:1 Cp$^b_2$ZrCl$_2$:Al^{i}Bu$_3$ ([Zr] = 150 μmol g$_{Al2O3}$$^{-1}$) evolve under the reaction conditions to give very active catalysts (8.4 × 10^7 g$_{PE}$ mol$_{Zr}$$^{-1}$ h^{-1}), but only 0.65 μmol Zr g$_{cat}$$^{-1}$ is adsorbed on the Al^{i}Bu$_3$/Al$_2$O$_3$ support. Contacting Al^{i}Bu$_3$ and Al$_2$O$_3$ results in the formation Al^{i}Bu$_3$/Al$_2$O$_3$ containing a distribution of Al–^{i}Bu sites on the alumina surface, but the organoaluminum sites are not effective activators of Cp$^b_2$ZrCl$_2$ in the absence of exogenous Al^{i}Bu$_3$ in solution. The excess alkylaluminum in solution reacts with Cp$^b_2$ZrCl$_2$ to form a mixture of zirconium hydrides,[155] of which only Cp$^b_2$Zr(μ-H)$_3$(Al^{i}Bu$_2$)(Al^{i}Bu$_3$) reacts with the Lewis sites on Al^{i}Bu$_3$/Al$_2$O$_3$ to form the active [Cp$_2$ZrH][HAlO$_X$]. The low surface coverage of [Cp$_2$ZrH][HAlO$_X$] is consistent with the expectation that only small quantities of strong Lewis acidic aluminum sites are accessible on γ-Al$_2$O$_3$.

Figure 12. Active species formed in reactions of Cp$^b_2$ZrCl$_2$, Al^{i}Bu$_3$, and Al$_2$O$_{3-600}$.

This ternary system is significantly more complex than reactions of discrete organometallics with partially dehydroxylated alumina, but they ultimately follow similar trends. These examples show that native Lewis acid sites on an oxide can also drive ion-pair formation, which is reasonable given the number of strong Lewis acids known to activate organometallics to form ion-pairs.[150, 156-163]

Halide Abstraction by R₃Si⁺ Containing Oxides

There are cases where the reactivity shown in eq 1 results in lower than expected surface coverage of well-defined sites. For example, the reaction of (α-diimine)Pd(CH₃)₂ with **SZO**, shown in Figure 13a, generates [(α-diimine)PdCH₃][**SZO**] but also more methane than expected. Only ~9 % of the electrophilic organopalladium sites present are active in polymerization reactions.[164] This result suggests that some Pd sites lack a Pd–CH₃ group required to polymerize olefins.
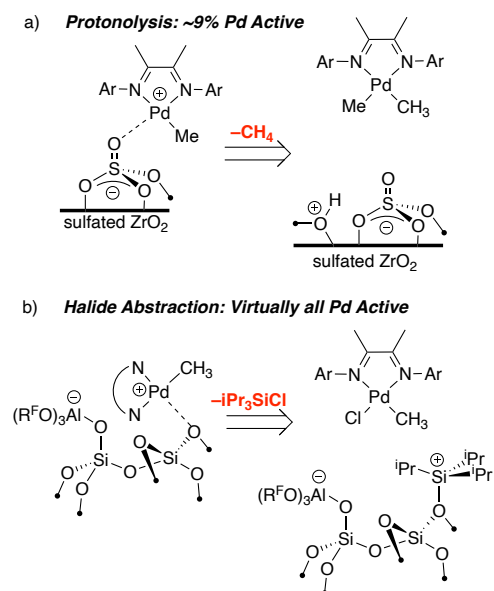

Figure 13. [(α-diimine)PdCH₃][**SZO**] polymerizes olefins with low active site counts (a); halide abstraction methodology with [ⁱPr₃Si][RᶠO₃Al–OSi≡] to form [(α-diimine)PdCH₃][RᶠO₃Al–OSi≡] (b).

More generally, the preparation of reactive organometallics is one of the bottlenecks preventing generation of well-defined sites on oxides. Indeed the most common method to generate an ion-pair in solution involves abstraction of a halide from a transition metal with, for example, a silver salt. Similar halide abstraction methods are not broadly available for surfaces, and is one of the reasons the protonolysis pathway shown in eq 1 dominates the field.

R₃Si⁺ ions are exceptionally strong Lewis acids with very high halide ion affinities. The reaction of [ⁱPr₃Si][RᶠO₃Al–OSi≡], which contains silylium-like ion fragments on the functionalized silica surface, reacts with (α-diimine)Pd(CH₃)Cl to form ⁱPr₃SiCl and [(α-diimine)PdCH₃][RᶠO₃Al–OSi≡] ion-pairs.[164] ⁱPr₃SiMe does not form in this reaction indicating that Pd–Me abstraction does not occur. From a coordination chemistry perspective, this halide abstraction methodology converts silica, a X-type or LX-type as discussed above, to a L-type ligand where the cationic palladium fragment interacts with siloxane bridge close to the [RᶠO₃Al–OSi≡] anion. Advanced solid-state NMR experiments support this arrangement. ¹³C{²⁷Al} Phase-Modulated Resonance-Echo Saturation-Pulse Double-Resonance (PM-RESPDOR)[165-167] experiments of [(α-diimine)PdCH₃][RᶠO₃Al–OSi≡] show that ¹³C NMR signals from the Pd-Me and the diimine ligand are not dipolar coupled to the ²⁷Al NMR signal, indicating that these spins are > ~5 Å from one another. ¹H{¹⁹F} Dipolar Heteronuclear Multiple Quantum Coherence (D-HMQC) NMR and ¹H–¹⁹F Symmetry-based Resonance-Echo Double-Resonance (S-REDOR) experiments[168] show that the

aromatic signals from [(α-diimine)PdCH₃][RᶠO₃Al–OSi≡] are close to the ¹⁹F NMR signal from [(RᶠO)₃Al–OSi≡)]. The experimental data fits to a Pd-Al internuclear distance a 11 Å, indicating that the [(N^N)Pd–CH₃]⁺ cation and the [(RᶠO)₃Al–OSi≡] anion are near yet weakly coordinated to each other on the surface.

The data shown in Figure 10 indicate that the sulfates on **SZO** are more coordinating (ie form stronger ion pairs) with cations than the [RᶠO₃Al–OSi≡] anion. This should affect the reactivity of the Pd–Me⁺ fragment in [(α-diimine)PdCH₃][RᶠO₃Al–OSi≡]. Indeed, reactions of [(α-diimine)Pd¹³CH₃][RᶠO₃Al–OSi≡] with vinyl chloride result in quantitative formation of propene,[169] indicating that all of the (α-diimine)Pd–¹³CH₃⁺ sites present on this material insert olefins, a significant improvement from the ~9% active Pd in [(α-diimine)PdCH₃][**SZO**]. [(α-diimine)Pd¹³CH₃][RᶠO₃Al–OSi≡] is as active as similar solution catalysts in olefin polymerization, but produces polymers with higher molecular weights, showing potential benefits of heterogenizing late-transition metal catalysts for this reaction. This halide abstraction methodology is in its infancy, but given the high halide ion affinity of R₃Si⁺ this method is expected to be fairly general.[156-163]

Coordination Chemistry on Carbon Surfaces

The chemistry of carbon surfaces with transition metals is significantly more limited than the examples described for oxides and offers an exciting platform for new inorganic chemistry. As discussed above, the π-extended graphene surface contains a superposition of e₂ᵤ-like and the e₁g-like frontier molecular orbitals (FMOs) that drive reactivity patterns of this material. Organic functionalization reactions of π-extended surfaces generally result in formation of sp³ carbons that disrupt the long range sp² conjugation and lead to poor conductivity and/or optical properties compared to pristine carbon nanomaterials.[29, 170] For example, real-time measurements on an individual carbon nanotube show that the formation of a single defect, i.e. sp³ center, increases the electrical resistance by ~6 kΩ.[171] In contrast, coordination of a transition metal to form an arene-like surface species is expected to preserve the sp² hybridization of the carbon atoms.

Reactions of highly oriented pyrolytic graphite (HOPG), graphene and single-walled carbon nanotubes (SWCNTs) with Cr(CO)₆ or (η⁶–benzene)Cr(CO)₃ form (η⁶–Cₙ)Cr(CO)₃, (η⁶– Cₙ)Cr(η⁶–C₆H₆) or (η⁶–Cₙ)₂Cr (Cₙ = π-conjugated carbon surface, Figure 14).[170] In these materials the e₁g and e₂ᵤ π-orbitals of graphene hybridize with the metal d-orbitals forming isolobal interactions similar to the stable 18 electron (η⁶-benzene)₂Cr or (η⁶-benzene)Cr(CO)₃. The product of these reactions depends on the dimensionality and the curvature of the carbon material. HOPG-reacts with Cr(CO)₆ to form (η⁶–HOPG)Cr(CO)₃, whereas reactions with single-layer graphene gave (η⁶–graphene)₂Cr. SWCNTs are less reactive than the flat materials due to the orbital effects as a result of curvature (Figure 2b).[172] Systematic studies of the effect of curvature on the coordination of transition metals are not available, but the reactivity of the carbon nanotubes should decrease as the nanotube diameter decreases due to orbital misalignment and reduced overlap with the transition metal. The smallest SWCNTs that form chromium complexes have diameters of 0.7 ~ 1 nm.
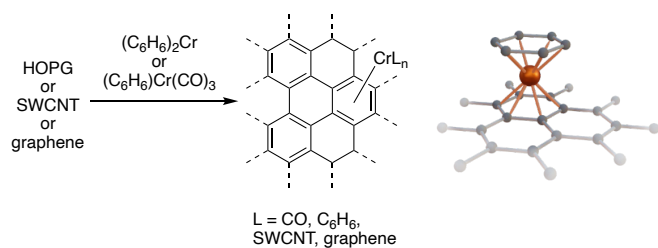
ARTICLE

Figure 14. Coordination of chromium complexes to carbon surfaces. A 3D model is shown next to the reaction to show the planarity of the hexagonal lattice of the carbon surface.

Raman and absorption spectroscopies provide a direct measurement of charge density distributions for carbon surfaces containing metals. Figure 15a shows the spectral characteristics of a pristine SWCNT film (black) as well as SWCNT films after deposition of elemental lithium (red) or after contacting with an appropriate chromium source (green).[173] The characteristic near infrared absorption bands related to the first (S_{11}) and second (S_{22}) interband transitions of semiconducting nanotubes are preserved in the Cr complexed SWCNTs, suggesting that Cr does not affect the band structure of the SWCNT. Depositing elemental lithium onto SWCNTs results in electron transfer into the conduction band (LUMO) of the SWCNT and significantly decreases these absorption features, indicating a drastic change in the electronic structure of the SWCNT. This electron transfer shifts the Fermi level of the nanotubes well into the van Hove singularities, which prevents interband transitions.
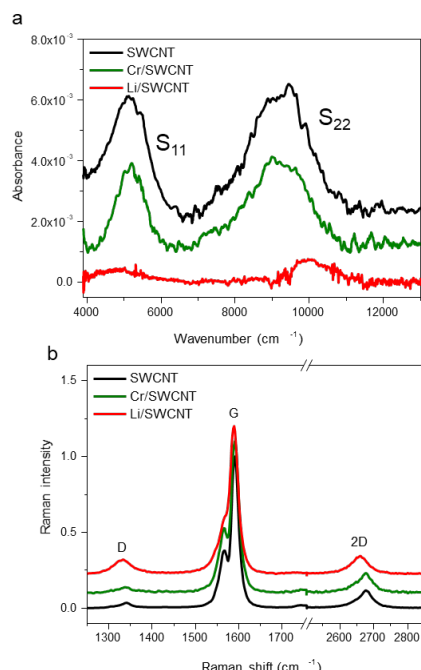

Figure 15. (a) Near infrared absorption spectra and (b) Raman spectra of SWCNT films: pristine (black curve), with chromium (green curve) and with lithium (red curve) deposition. Modified from ref 173. Copyright 2014 American Chemical Society.

Raman spectroscopy is a very common analytical method in studies of carbon materials. Figure 15b shows Raman spectra for pristine SWCNTs (black), chromium containing SWCNTs (green),

and lithium doped SWCNTs (red).[173] The 2D Raman band in nanocarbon materials is sensitive to charge transfer. Figure 15b shows that the 2D band in pristine SWCNTs and Cr/SWCNT materials are essentially identical, indicating that the interaction between Cr and the extended π-surface in SWNTs is not related to significant charge transfer and the bonding is covalent rather than ionic. This is not the case in Li/SWCNT materials that have a significantly red-shifted 2D band in the Raman spectra (Figure 15b, red spectrum), indicating charge transfer between lithium and the LUMO of the SWCNT.

The preservation of the extended π-system in these "organometallic" graphene and SWCNTs results in materials that have interesting electronic properties that is consistent with the proposed (η⁶-C_n)M. For example, thin films of interconnected semiconducting SWCNTs bridged with (η⁶-C_n)Cr interconnects are *700,000 times* more conductive than the pristine semiconducting SWCNT film.[173] Aligned carbon nanotube films similarly form (η⁶–C_n)₂M,[174, 175] which is important because the extraordinary electronic properties of individual SWCNTs are often lost in random network or bundled (aggregated) SWCNTs.

The dramatic increase in conductivity is related to the formation of stable (η⁶-C_n)₂Cr units with high density of states (DOS) near the Fermi level which open new conducting channels facilitating electron transport across the π-conjugated carbon surfaces. Figure 16 shows these effects for aligned SWCNTs containing (η⁶-C_n)₂Cr (left) or doped with elemental lithium (right). There is an element dependent increase in intratube or intertube conductivity. Li doping enhances the conductivity along the nanotube (intratube), but Cr increases the intertube transport. This is consistent with the spectroscopy in Figure 15 showing that Li transfers electrons to the LUMO of the SWCNTs (0.175 e⁻ per Li atom). Though this charge transfer is responsible for the increased intratube conductivity of the SWCNT, there is no beneficial intertube conductivity in Li doped SWCNTs.

In η⁶-(C_n)Cr the intertube conductivity increases significantly. The high density of states (DOS) near the Fermi level (Figure 15b) of the Cr-SWNT are related to the electronic states from the Cr atom that hybridize with the C atoms on the SWCNT and form conducting channels between SWCNTs.[172, 186] Figure 16d shows the total electron density for a Cr/SWCNT containing (η⁶-C_n)Cr units. The electron density from chromium overlaps with the SWCNTs and increases intertube transport. Similar electronic overlap is not observed with lithium (Figure 16h).
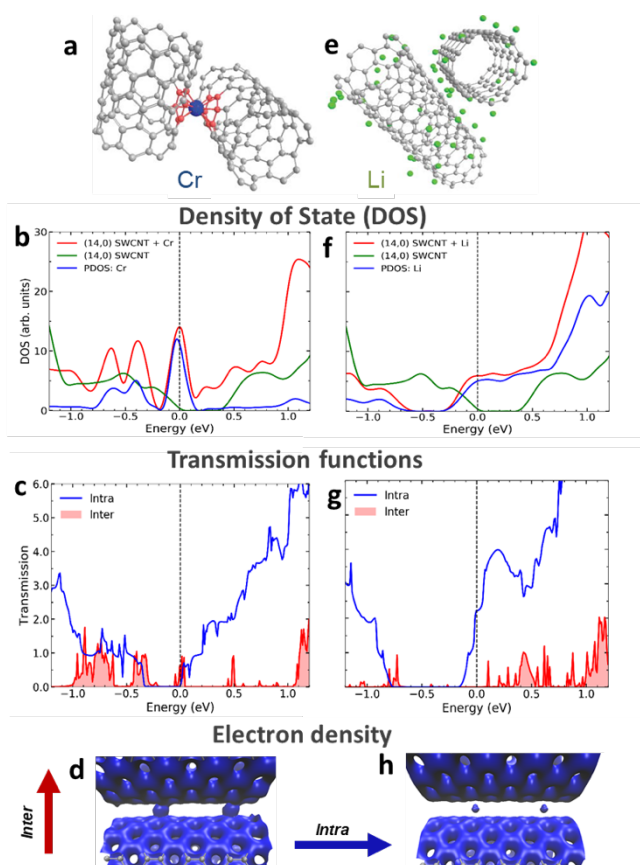
ARTICLE

Figure 15. Single-wall carbon nanotube (SWCNT) interactions with metal atoms: (a) Cr and (b) lithium. (c,d) Density of states (DOS) for (c) Cr-SWCNTs and (d) Li-SWCNTs along with the projected DOS for each metal atom (green). (e,f) Intertube (red) and intratube (blue) electronic transmission functions for SWCNT junctions with added Cr (e) and Li (f) compared to pristine (14,0) SWCNTs (green). (g,h) Total electron density (blue iso-surface) of $(\eta^6\text{-SWCNT})_2\text{Cr}$ and Li-doped SWCNTs. Reprinted with permission from ref 175. Copyright 2019 American Chemical Society.

DFT methods suggest that formation of $(\eta^6\text{-C}_n)_2\text{M}$ should be somewhat general.[176, 177] Indeed, complexes of graphene and SWCNTs were synthesized with Mo and W,[178] first row metals (Ti, V, Cr, Mn, Fe),[23] and the lanthanides (Ln = Sm, Eu, Gd, Dy, Ho, Yb).[179, 180] However, not all carbon nanomaterials form similar $(\eta^6\text{-C}_n)_2\text{M}$ interconnects. For example, orbital misalignment in fullerenes prevents formation of $(\eta^6\text{-C}_n)_2\text{M}$ interconnects described above.[181-185]

Outlook

The ability to rationally control structure at the molecular level suffused the field of inorganic chemistry since its inception.[186] In this context, perhaps it is not surprising that design strategies would emerge to form well-defined sites on extended surfaces. What is surprising is the reductionist principles developed for small molecules in solution overlap so recognizably with design strategies to obtain well-defined sites on surfaces. The extent of the relationship remains to be developed, particularly in cases where material interfaces are

specifically engineered to contain a ligand to coordinate to a transition metal,[187-190] but if past is prologue the insights provided by the molecular chemistry community will continue to impact the atomistic design of structurally defined sites on surfaces for a range of applications.

Author Contributions

Both authors contributed to the preparation of this manuscript.

Conflicts of interest

There are no conflicts to declare.

Acknowledgements

Notes and references

1.   *Handbook of Heterogeneous Catalysis*, Wiley-VCH, 1st edn., 1997.
2.   M. S. Strano, C. A. Dyke, M. L. Usrey, P. W. Barone, M. J. Allen, H. Shan, C. Kittrell, R. H. Hauge, J. M. Tour and R. E. Smalley, *Science*, 2003, **301**, 1519-1522.
3.   C. A. Dyke and J. M. Tour, *J. Phys. Chem. A*, 2004, **108**, 11151-11159.
4.   D. Tasis, N. Tagmatarchis, A. Bianco and M. Prato, *Chem. Rev.*, 2006, **106**, 1105-1136.
5.   M. Endo, M. S. Strano and P. M. Ajayan, *Carbon Nanotubes*, 2008, **111**, 13-61.
6.   M. J. Allen, V. C. Tung and R. B. Kaner, *Chem. Rev.*, 2010, **110**, 132-145.
7.   G. S. Hong, S. O. Diao, A. L. Antaris and H. J. Dai, *Chem. Rev.*, 2015, **115**, 10816-10906.
8.   B. Wang, C. G. Hua and L. M. Dai, *Chem. Comm.*, 2016, **52**, 14350-14360.
9.   M. N. Jackson and Y. Surendranath, *Acc. Chem. Res.*, 2019, **52**, 3432-3441.
10.   E. Bekyarova, S. Sarkar, F. Wang, M. E. Itkis, I. Kalinina, X. Tian and R. C. Haddon, *Acc. Chem. Res.*, 2013, **46**, 65-76.
11.   C. A. Tolman, *Chem. Rev.*, 1977, **77**, 313-348.
12.   L. Falivene, R. Credendino, A. Poater, A. Petta, L. Serra, R. Oliva, V. Scarano and L. Cavallo, *Organometallics*, 2016, **35**, 2286-2293.
13.   S. Maier, S. P. Cronin, M.-A. Vu Dinh, Z. Li, M. Dyballa, M. Nowakowski, M. Bauer and D. P. Estes, *Organometallics*, 2021, **40**, 1751-1757.
14.   T. J. Marks, *Acc. Chem. Res.*, 1992, **25**, 57-65.
15.   S. L. Wegener, T. J. Marks and P. C. Stair, *Acc. Chem. Res.*, 2011, **45**, 206-214.
16.   M. Stalzer, M. Delferro and T. Marks, *Catal. Lett.*, 2015, **145**, 3-14.
17.   J.-M. Basset, C. Coperet, D. Soulivong, M. Taoufik and J. T. Cazat, *Acc. Chem. Res.*, 2009, **43**, 323-334.

18. C. Copéret, M. Chabanas, R. Petroff Saint-Arroman and J.-M. Basset, *Angew. Chem., Int. Ed.*, 2003, **42**, 156-181.

19. J. Guzman and B. C. Gates, *Dalton Trans.*, 2003, DOI: 10.1039/b303285j, 3303-3318.

20. R. L. Brutchey and T. D. Tilley, *Top. Organomet. Chem.*, 2005, 69-115.

21. Y. Liang and R. Anwander, *Dalton Trans.*, 2013, **42**, 12521-12545.

22. R. J. Witzke, A. Chapovetsky, M. P. Conley, D. M. Kaphan and M. Delferro, *ACS Catal.*, 2020, DOI: 10.1021/acscatal.0c03350, 11822-11840.

23. F. Wang, M. E. Itkis, E. B. Bekyarova, X. Tian, S. Sarkar, A. Pekker, I. Kalinina, M. L. Moser and R. C. Haddon, *Appl. Phys. Lett.*, 2012, **100**, 223111.

24. F. Wang, M. E. Itkis, E. Bekyarova, S. Sarkar, X. Tian and R. C. Haddon, *J. Phys. Org. Chem.*, 2012, **25**, 607-610.

25. A. H. Castro Neto, F. Guinea, N. M. R. Peres, K. S. Novoselov and A. K. Geim, *Rev. Mod. Phys.*, 2009, **81**, 109-162.

26. M.-H. Whangbo, R. Hoffmann and R. B. Woodward, *Proc. Royal Soc. Lond. A*, 1979, **366**, 23-46.

27. S. Sarkar, E. Bekyarova and R. C. Haddon, *Acc. Chem. Res.*, 2012, **45**, 673-682.

28. E. B. Bekyarova, S. Niyogi, S. Sarkar, X. Tian, M. Chen, M. L. Moser, K. Ayub, R. H. Mitchell and R. C. Haddon, *Synth. Met.*, 2015, **210**, 80-84.

29. S. Niyogi, M. A. Hamon, H. Hu, B. Zhao, P. Bhowmik, R. Sen, M. E. Itkis and R. C. Haddon, *Acc. Chem. Res.*, 2002, **35**, 1105-1113.

30. M. A. Hamon, M. E. Itkis, S. Niyogi, T. Alvaraez, C. Kuper, M. Menon and R. C. Haddon, *J. Am. Chem. Soc.*, 2001, **123**, 11292-11293.

31. S. Banerjee and S. S. Wong, *Nano Lett.*, 2002, **2**, 49-53.

32. S. Banerjee and S. S. Wong, *J. Am. Chem. Soc.*, 2002, **124**, 8940-8948.

33. L. Meng, C. Fu, Z. Fei, Q. Lu and P. J. Dyson, *Inorg. Chim. Acta*, 2010, **363**, 3926-3931.

34. L. T. Zhuravlev, *Colloids and Surfaces A: Physicochemical and Engineering Aspects*, 2000, **173**, 1-38.

35. M. L. H. Green and G. Parkin, *J. Chem. Educ.*, 2014, **91**, 807-816.

36. K. A. Reid and D. C. Powers, *Chem. Commun.*, 2021, **57**, 4993-5003.

37. F. A. Perras, U. Kanbur, A. L. Paterson, P. Chatterjee, I. I. Slowing and A. D. Sadow, *Inorg. Chem.*, 2022, **61**, 1067-1078.

38. F. A. Perras, A. L. Paterson, Z. H. Syed, A. J. Kropf, D. M. Kaphan, M. Delferro and M. Pruski, *J. Phys. Chem. C*, 2021, **125**, 13433-13442.

39. A. L. Paterson, D.-J. Liu, U. Kanbur, A. D. Sadow and F. A. Perras, *Inorganic Chemistry Frontiers*, 2021, **8**, 1416-1431.

40. E. Le Roux, M. Chabanas, A. Baudouin, A. de Mallmann, C. Copéret, E. A. Quadrelli, J. Thivolle-Cazat, J.-M. Basset, W. Lukens, A. Lesage, L. Emsley and G. J. Sunley, *J. Am. Chem. Soc.*, 2004, **126**, 13391-13399.

41. B. Rhers, A. Salameh, A. Baudouin, E. A. Quadrelli, M. Taoufik, C. Copéret, F. Lefebvre, J.-M. Basset, X. Solans-Monfort, O. Eisenstein, W. W. Lukens, L. P. H. Lopez, A. Sinha and R. R. Schrock, *Organometallics*, 2006, **25**, 3554-3557.

42. M. Chabanas, A. Baudouin, C. Copéret, J.-M. Basset, W. Lukens, A. Lesage, S. Hediger and L. Emsley, *J. Am. Chem. Soc.*, 2002, **125**, 492-504.

43. E. Mazoyer, N. Merle, A. d. Mallmann, J.-M. Basset, E. Berrier, L. Delevoye, J.-F. Paul, C. P. Nicholas, R. M. Gauvin and M. Taoufik, *Chem. Commun.*, 2010, **46**, 8944-8946.

44. M. P. Conley, G. Lapadula, K. Sanders, D. Gajan, A. Lesage, I. del Rosal, L. Maron, W. W. Lukens, C. Copéret and R. A. Andersen, *J. Am. Chem. Soc.*, 2016, **138**, 3831-3843.

45. Y. Chen, E. Callens, E. Abou-Hamad, N. Merle, A. J. P. White, M. Taoufik, C. Coperet, E. Le Roux and J. M. Basset, *Angew. Chem., Int. Ed.*, 2012, **51**, 11886-11889.

46. A. Saidi, W. Al Maksoud, M. K. Samantaray, E. Abou-Hamad and J.-M. Basset, *Chem. Commun.*, 2020, **56**, 13401-13404.

47. N. Merle, J. Tr√©bosc, A. Baudouin, I. D. Rosal, L. Maron, K. Szeto, M. Genelot, A. Mortreux, M. Taoufik, L. Delevoye and R. g. M. Gauvin, *J. Am. Chem. Soc.*, 2012, **134**, 9263-9275.

48. J. Autschbach, S. Zheng and R. W. Schurko, *Conc. Mag. Res. A*, 2010, **36A**, 84-126.

49. T. Vancompernolle, X. Trivelli, L. Delevoye, F. Pourpoint and R. M. Gauvin, *Dalton Trans.*, 2017, **46**, 13176-13179.

50. D. B. Culver, W. Huynh, H. Tafazolian and M. P. Conley, *Organometallics*, 2020, **39**, 1112-1122.

51. D. B. Culver, W. Huynh, H. Tafazolian, T.-C. Ong and M. P. Conley, *Angew. Chem., Int. Ed.*, 2018, **57**, 9520-9523.

52. W. Huynh, D. B. Culver, H. Tafazolian and M. P. Conley, *Dalton Trans.*, 2018, **47**, 13063-13071.

53. T. Vancompernolle, N. Merle, F. Capet, I. Del Rosal, M. Laurent, L. Delevoye, F. Pourpoint and R. M. Gauvin, *Dalton Trans.*, 2019, **48**, 5243-5252.

54. A. G. Avent, C. F. Caro, P. B. Hitchcock, M. F. Lappert, Z. Li and X.-H. Wei, *Dalton Trans.*, 2004, DOI: 10.1039/b316695n, 1567-1577.

55. P. B. Hitchcock, M. F. Lappert, R. G. Smith, R. A. Bartlett and P. P. Power, *Chem. Commun.*, 1988, DOI: 10.1039/c39880001007, 1007-1009.

56. N. Eedugurala, Z. Wang, K. Yan, K. C. Boteju, U. Chaudhary, T. Kobayashi, A. Ellern, I. I. Slowing, M. Pruski and A. D. Sadow, *Organometallics*, 2017, **36**, 1142-1153.

57. A. Pindwal, K. Yan, S. Patnaik, B. M. Schmidt, A. Ellern, I. I. Slowing, C. Bae and A. D. Sadow, *J. Am. Chem. Soc.*, 2017, **139**, 16862-16874.

58. Z. Wang, S. Patnaik, N. Eedugurala, J. S. Manzano, I. I. Slowing, T. Kobayashi, A. D. Sadow and M. Pruski, *J. Am. Chem. Soc.*, 2020, **142**, 2935-2947.

59. J. D. A. Pelletier and J.-M. Basset, *Acc. Chem. Res.*, 2016, **49**, 664-677.

60. N. Maity, S. Barman, E. Callens, M. K. Samantaray, E. Abou-Hamad, Y. Minenkov, V. D'Elia, A. S. Hoffman, C. M. Widdifield, L. Cavallo, B. C. Gates and J.-M. Basset, *Chem. Sci.*, 2016, **7**, 1558-1568.

61. F. Rataboul, A. Baudouin, C. Thieuleux, L. Veyre, C. Copéret, J. Thivolle-Cazat, J.-M. Basset, A. Lesage and L. Emsley, *J. Am. Chem. Soc.*, 2004, **126**, 12541-12550.

62. V. A. Zakharov, V. K. Dudchenko, E. A. Paukshtis, L. G. Karakchiev and Y. I. Yermakov, *J. Mol. Catal.*, 1977, **2**, 421-435.

63. Y. Chen, E. Abou-hamad, A. Hamieh, B. Hamzaoui, L. Emsley and J.-M. Basset, *J. Am. Chem. Soc.*, 2015, **137**, 588-591.

64. M. K. Samantaray, E. Callens, E. Abou-Hamad, A. J. Rossini, C. M. Widdifield, R. Dey, L. Emsley and J.-M. Basset, *J. Am. Chem. Soc.*, 2014, **136**, 1054-1061.

65. N. Popoff, R. M. Gauvin, M. A. De and M. Taoufik, *Organometallics*, 2012, **31**, 4763-4768.

66. A. Kermagoret, R. N. Kerber, M. P. Conley, E. Callens, P. Florian, D. Massiot, C. Coperet, F. Delbecq, X. Rozanska and P. Sautet, *Dalton Trans.*, 2013, **42**, 12681-12687.

67. R. N. Kerber, A. Kermagoret, E. Callens, P. Florian, D. Massiot, A. Lesage, C. Copéret, F. ß. Delbecq, X. Rozanska and P. Sautet, *J. Am. Chem. Soc.*, 2012, **134**, 6767-6775.

68. A. Kermagoret, R. N. Kerber, M. P. Conley, E. Callens, P. Florian, D. Massiot, F. ß. Delbecq, X. Rozanska, C. Cop√ ©ret and P. Sautet, *J. Catal.*, 2014, **313**, 46-54.

69. I. B. Moroz, P. Florian, J. Viger-Gravel, C. P. Gordon, A. Lesage and C. Copéret, *Angew. Chem., Int. Ed.*, 2020, **59**, 16167-16172.

70. M. A. Bashir, T. Vancompernolle, R. M. Gauvin, L. Delevoye, N. Merle, V. Monteil, M. Taoufik, T. F. L. McKenna and C. Boisson, *Cat. Sci. Tech.*, 2016, **6**, 2962-2974.

71. D. W. Sauter, N. Popoff, M. A. Bashir, K. C. Szeto, R. M. Gauvin, L. Delevoye, M. Taoufik and C. Boisson, *Chem. Commun.*, 2016, **52**, 4776-4779.

72. J. Pelletier, J. Espinas, N. Vu, S. Norsic, A. Baudouin, L. Delevoye, J. Trébosc, E. Le Roux, C. Santini, J.-M. Basset, R. M. Gauvin and M. Taoufik, *Chem. Commun.*, 2011, **47**, 2979-2981.

73. D. W. Sauter, V. Chiari, N. Aykac, S. Bouaouli, L. Perrin, L. Delevoye, R. M. Gauvin, K. C. Szeto, C. Boisson and M. Taoufik, *Dalton Trans.*, 2017, **46**, 11547-11551.

74. S. D. Fleischman and S. L. Scott, *J. Am. Chem. Soc.*, 2011, **133**, 4847-4855.

75. Z. A. Taha, E. W. Deguns, S. Chattopadhyay and S. L. Scott, *Organometallics*, 2006, **25**, 1891-1899.

76. K. C. Szeto, Z. R. Jones, N. Merle, C. Rios, A. Gallo, F. Le Quemener, L. Delevoye, R. M. Gauvin, S. L. Scott and M. Taoufik, *ACS Catal.*, 2018, **8**, 7566-7577.

77. M. P. Conley, A. J. Rossini, A. Comas-Vives, M. Valla, G. Casano, O. Ouari, P. Tordo, A. Lesage, L. Emsley and C. Copéret, *Phys. Chem. Chem. Phys.*, 2014, **16**, 17822-17827.

78. V. Dufaud and J.-M. Basset, *Angew. Chem., Int. Ed.*, 1998, **37**, 806-810.

79. U. Kanbur, G. Zang, A. L. Paterson, P. Chatterjee, R. A. Hackler, M. Delferro, I. I. Slowing, F. A. Perras, P. Sun and A. D. Sadow, *Chem*, 2021, **7**, 1347-1362.

80. C. Copéret, Z. J. Berkson, K. W. Chan, J. de Jesus Silva, C. P. Gordon, M. Pucino and P. A. Zhizhko, *Chem. Sci.*, 2021, **12**, 3092-3115.

81. M. Chabanas, A. Baudouin, C. Copéret and J.-M. Basset, *J. Am. Chem. Soc.*, 2001, **123**, 2062-2063.

82. X. Solans-Monfort, E. Clot, C. Copéret and O. Eisenstein, *J. Am. Chem. Soc.*, 2005, **127**, 14015-14025.

83. A. H. Hoveyda, Z. Liu, C. Qin, T. Koengeter and Y. Mu, *Angew. Chem., Int. Ed.*, 2020, **59**, 22324-22348.

84. M. M. Flook, A. J. Jiang, R. R. Schrock, P. Müller and A. H. Hoveyda, *J. Am. Chem. Soc.*, 2009, **131**, 7962-7963.

85. E. M. Townsend, R. R. Schrock and A. H. Hoveyda, *J. Am. Chem. Soc.*, 2012, **134**, 11334-11337.

86. D. V. Peryshkov, W. P. Forrest, R. R. Schrock, S. J. Smith and P. Müller, *Organometallics*, 2013, **32**, 5256-5259.

87. M. P. Conley, W. P. Forrest, V. Mougel, C. Copéret and R. R. Schrock, *Angew. Chem., Int. Ed.*, 2014, **53**, 14221-14224.

88. L. P. H. Lopez, R. R. Schrock and P. Muller, *Organometallics*, 2006, **25**, 1978-1986.

89. R. R. Schrock, *Chem. Rev.*, 2009, **109**, 3211-3226.

90. D. L. Nascimento, M. Foscato, G. Occhipinti, V. R. Jensen and D. E. Fogg, *J. Am. Chem. Soc.*, 2021, **143**, 11072-11079.

91. S. Lassalle, R. Jabbour, P. Schiltz, P. Berruyer, T. K. Todorova, L. Veyre, D. Gajan, A. Lesage, C. Thieuleux and C. Camp, *J. Am. Chem. Soc.*, 2019, **141**, 19321-19335.

92. A. Macchioni, *Chem. Rev.*, 2005, **105**, 2039-2074.

93. D. M. Kaphan, R. C. Klet, F. A. Perras, M. Pruski, C. Yang, A. J. Kropf and M. Delferro, *ACS Catal.*, 2018, **8**, 5363-5373.

94. E. S. Stoyanov, K.-C. Kim and C. A. Reed, *J. Am. Chem. Soc.*, 2006, **128**, 8500-8508.

95. A. B. A. Rupp and I. Krossing, *Acc. Chem. Res.*, 2015, **48**, 2537-2546.

96. I. M. Riddlestone, A. Kraft, J. Schaefer and I. Krossing, *Angew. Chem., Int. Ed.*, 2018, **57**, 13982-14024.

97. R. J. Gorte, *Catal. Lett.*, 1999, **62**, 1-13.

98. J. Rodriguez, D. B. Culver and M. P. Conley, *J. Am. Chem. Soc.*, 2019, **141**, 1484-1488.

99. A. Zheng, S.-B. Liu and F. Deng, *Chem. Rev.*, 2017, **117**, 12475-12531.

100. X. Yi, Y.-K. Peng, W. Chen, Z. Liu and A. Zheng, *Acc. Chem. Res.*, 2021, **54**, 2421-2433.

101. F. Haase and J. Sauer, *J. Am. Chem. Soc.*, 1998, **120**, 13503-13512.

102. A. A. Viggiano, M. J. Henchman, F. Dale, C. A. Deakyne and J. F. Paulson, *J. Am. Chem. Soc.*, 1992, **114**, 4299-4306.

103. J. Sauer and R. Ahlrichs, *J. Chem. Phys.*, 1990, **93**, 2575-2583.

104. H. Yamamoto and K. Futatsugi, *Angew. Chem., Int. Ed.*, 2005, **44**, 1924-1942.

105. G. A. Olah, G. K. S. Prakash, J. Sommer and A. Molnar, *Superacid Chemistry*, John Wiley & sons, 2009.

106. L. O. Müller, D. Himmel, J. Stauffer, G. Steinfeld, J. Slattery, G. Santiso-Quiñones, V. Brecht and I. Krossing, *Angew. Chem., Int. Ed.*, 2008, **47**, 7659-7663.

107. D. B. Culver, A. Venkatesh, W. Huynh, A. J. Rossini and M. P. Conley, *Chem. Sci.*, 2020, **11**, 1510 - 1517.

108. A. Kraft, J. Beck, G. Steinfeld, H. Scherer, D. Himmel and I. Krossing, *Organometallics*, 2012, **31**, 7485-7491.

109. H. F. T. Klare, L. Albers, L. Süsse, S. Keess, T. Müller and M. Oestreich, *Chem. Rev.*, 2021, **121**, 5889-5985.

110. C. A. Reed, *Acc. Chem. Res.*, 1998, **31**, 325-332.

111. C. A. Reed, *Acc. Chem. Res.*, 2010, **43**, 121-128.

112. K.-C. Kim, C. A. Reed, D. W. Elliott, L. J. Mueller, F. Tham, L. Lin and J. B. Lambert, *Science*, 2002, **297**, 825-827.

113. Z. Xie, J. Manning, R. W. Reed, R. Mathur, P. D. W. Boyd, A. Benesi and C. A. Reed, *J. Am. Chem. Soc.*, 1996, **118**, 2922-2928.

114. C. A. Reed, Z. Xie, R. Bau and A. Benesi, *Science*, 1993, **262**, 402-404.

115. W. Huynh and M. P. Conley, *Dalton Trans.*, 2020, **49**, 16453-16463.

116. D. B. Culver and M. P. Conley, *Angew. Chem., Int. Ed.*, 2018, **57**, 14902-14905.

117. T. Deschner, Y. Liang and R. Anwander, *J. Phys. Chem. C*, 2010, **114**, 22603-22609.

118. C. Zapilko, M. Widenmeyer, I. Nagl, F. Estler, R. Anwander, G. Raudaschl-Sieber, O. Groeger and G. Engelhardt, *J. Am. Chem. Soc.*, 2006, **128**, 16266-16276.

119. J. Bluemel, *J. Am. Chem. Soc.*, 1995, **117**, 2112-2113.

120. M. Ahrens, G. Scholz, T. Braun and E. Kemnitz, *Angew. Chem., Int. Ed.*, 2013, **52**, 5328-5332.

121. V. J. Scott, R. Celenligil-Cetin and O. V. Ozerov, *J. Am. Chem. Soc.*, 2005, **127**, 2852-2853.
122. C. Douvris and O. V. Ozerov, *Science*, 2008, **321**, 1188-1190.
123. G. Busca, *Catal. Today*, 2014, **226**, 2-13.
124. C. Morterra and G. Magnacca, *Catal. Today*, 1996, **27**, 497-532.
125. R. Wischert, C. Coperet, F. Delbecq and P. Sautet, *Chem. Commun.*, 2011, **47**, 4890-4892.
126. S. A. Zubkov, V. Y. Borovkov, S. G. Gagarin and V. B. Kazansky, *Chem. Phys. Lett.*, 1984, **107**, 337-340.
127. R. Wischert, C. Copéret, F. Delbecq and P. Sautet, *Angew. Chem., Int. Ed.*, 2011, **50**, 3202-3205.
128. K. Khivantsev, N. R. Jaegers, J.-H. Kwak, J. Szanyi and L. Kovarik, *Angew. Chem., Int. Ed.*, 2021, **60**, 17522-17530.
129. R. Wischert, P. Laurent, C. Copéret, F. Delbecq and P. Sautet, *J. Am. Chem. Soc.*, 2012, **134**, 14430-14449.
130. D. G. H. Ballard, *Journal of Polymer Science: Polymer Chemistry Edition*, 1975, **13**, 2191-2212.
131. D. G. H. Ballard, E. Jones, R. J. Wyatt, R. T. Murray and P. A. Robinson, *Polymer*, 1974, **15**, 169-174.
132. D. G. H. Ballard, in *Adv. Catal.*, eds. H. P. D.D. Eley and B. W. Paul, Academic Press, 1973, vol. Volume 23, pp. 263-325.
133. Y. I. Yermakov, in *Stud. Surf. Sci. Catal.*, eds. T. Seivama and K. Tanabe, Elsevier, 1981, vol. Volume 7, Part A, pp. 57-76.
134. P. J. Toscano and T. J. Marks, *J. Am. Chem. Soc.*, 1985, **107**, 653-659.
135. M. Jezequel, V. Dufaud, M. J. Ruiz-Garcia, F. Carrillo-Hermosilla, U. Neugebauer, G. P. Niccolai, F. Lefebvre, F. Bayard, J. Corker, S. Fiddy, J. Evans, J.-P. Broyer, J. Malinge and J.-M. Basset, *J. Am. Chem. Soc.*, 2001, **123**, 3520-3540.
136. J. Joubert, F. Delbecq, P. Sautet, E. Le Roux, M. Taoufik, C. Thieuleux, F. Blanc, C. Coperet, J. Thivolle-Cazat and J. M. Basset, *J. Am. Chem. Soc.*, 2006, **128**, 9157-9169.
137. M. Delgado, C. C. Santini, F. o. Delbecq, R. l. Wischert, B. L. Guennic, G. r. Tosin, R. Spitz, J.-M. Basset and P. Sautet, *J. Phys. Chem. C*, 2010, **114**, 18516-18528.
138. M. Delgado, F. Delbecq, C. C. Santini, F. Lefebvre, S. Norsic, P. Putaj, P. Sautet and J.-M. Basset, *J. Phys. Chem. C*, 2012, **116**, 834-843.
139. M. Taoufik, E. Le Roux, J. Thivolle-Cazat, C. Copéret, J.-M. Basset, B. Maunders and G. J. Sunley, *Top. Catal.*, 2006, **40**, 65-70.
140. H. Ahn and T. J. Marks, *J. Am. Chem. Soc.*, 2002, **124**, 7103-7110.
141. E. Le Roux, M. Taoufik, C. Coperet, A. de Mallmann, J. Thivolle-Cazat, J. M. Basset, B. M. Maunders and G. J. Sunley, *Angew. Chem. Int. Ed.*, 2005, **44**, 6755-6758.
142. W. P. Long and D. S. Breslow, *J. Am. Chem. Soc.*, 1960, **82**, 1953-1957.
143. S. Xu and E.-i. Negishi, *Acc. Chem. Res.*, 2016, **49**, 2158-2168.
144. W. Kaminsky, *Dalton Trans.*, 1998, DOI: 10.1039/a800056e, 1413-1418.
145. R. F. Jordan, C. S. Bajgur, R. Willett and B. Scott, *J. Am. Chem. Soc.*, 1986, **108**, 7410-7411.
146. R. F. Jordan, W. E. Dasher and S. F. Echols, *J. Am. Chem. Soc.*, 1986, **108**, 1718-1719.
147. G. G. Hlatky, H. W. Turner and R. R. Eckman, *J. Am. Chem. Soc.*, 1989, **111**, 2728-2729.
148. X. Yang, C. L. Stern and T. J. Marks, *J. Am. Chem. Soc.*, 1994, **116**, 10015-10031.
149. X. Yang, C. L. Stern and T. J. Marks, *Angewandte Chemie International Edition in English*, 1992, **31**, 1375-1377.
150. E. Y.-X. Chen and T. J. Marks, *Chem. Rev.*, 2000, **100**, 1391-1434.
151. M. Bochmann and S. J. Lancaster, *Angewandte Chemie International Edition in English*, 1994, **33**, 1634-1637.
152. M. P. McDaniel, M. D. Jensen, K. Jayaratne, K. S. Collins, E. A. Benham, N. D. Mcdaniel, P. K. Das, J. L. Martin, Q. Yang, M. G. Thorn and A. P. Masino, in *Tailor-Made Polymers*, eds. J. R. Severn and J. C. Chadwick, 2008, DOI: 10.1002/9783527621668.ch7, pp. 171-210.
153. S. Collins, W. M. Kelly and D. A. Holden, *Macromolecules*, 1992, **25**, 1780-1785.
154. D. B. Culver, R. W. Dorn, A. Venkatesh, J. Meeprasert, A. J. Rossini, E. A. Pidko, A. S. Lipton, G. R. Lief and M. P. Conley, *ACS Cent. Sci.*, 2021, **7**, 1225-1231.
155. D. B. Culver, J. Corieri, G. Lief and M. P. Conley, *Organometallics*, 2022, **41**, 892-899.
156. C. Douvris and C. A. Reed, *Organometallics*, 2008, **27**, 807-810.
157. F.-S. Guo, Y.-C. Chen, M.-L. Tong, A. Mansikkamäki and R. A. Layfield, *Angew. Chem., Int. Ed.*, 2019, **58**, 10163-10167.
158. F.-S. Guo, B. M. Day, Y.-C. Chen, M.-L. Tong, A. Mansikkamäki and R. A. Layfield, *Science*, 2018, **362**, 1400-1403.
159. C. A. P. Goodwin, D. Reta, F. Ortu, N. F. Chilton and D. P. Mills, *J. Am. Chem. Soc.*, 2017, **139**, 18714-18724.
160. H. M. Nicholas, M. Vonci, C. A. P. Goodwin, S. W. Loo, S. R. Murphy, D. Cassim, R. E. P. Winpenny, E. J. L. McInnes, N. F. Chilton and D. P. Mills, *Chem. Sci.*, 2019, **10**, 10493-10502.
161. C. A. P. Goodwin, F. Ortu, D. Reta, N. F. Chilton and D. P. Mills, *Nature*, 2017, **548**, 439-442.
162. F.-S. Guo, B. M. Day, Y.-C. Chen, M.-L. Tong, A. Mansikkamäki and R. A. Layfield, *Angew. Chem., Int. Ed.*, 2017, **56**, 11445-11449.
163. V. Varga, M. Lamač, M. Horáček, R. Gyepes and J. Pinkas, *Dalton Trans.*, 2016, **45**, 10146-10150.
164. J. Gao, R. W. Dorn, G. P. Laurent, F. A. Perras, A. J. Rossini and M. P. Conley, *Angew. Chem., Int. Ed.*, 2022, **n/a**, e202117279.
165. Z. Gan, *Chem. Commun.*, 2006, DOI: 10.1039/B611447D, 4712-4714.
166. L. Chen, Q. Wang, B. Hu, O. Lafon, J. Trébosc, F. Deng and J.-P. Amoureux, *Phys. Chem. Chem. Phys.*, 2010, **12**, 9395-9405.
167. E. Nimerovsky, R. Gupta, J. Yehl, M. Li, T. Polenova and A. Goldbourt, *J. Magn. Reson.*, 2014, **244**, 107-113.
168. A. Brinkmann and A. P. M. Kentgens, *J. Am. Chem. Soc.*, 2006, **128**, 14758-14759.
169. S. M. Kilyanek, E. J. Stoebenau, N. Vinayavekhin and R. F. Jordan, *Organometallics*, 2010, **29**, 1750-1760.
170. D. Tasis, N. Tagmatarchis, A. Bianco and M. Prato, *Chem. Rev.*, 2006, **106**, 1105-1136.
171. H. Wilson, S. Ripp, L. Prisbrey, M. A. Brown, T. Sharf, D. J. T. Myles, K. G. Blank and E. D. Minot, *J. Phys. Chem. C*, 2016, **120**, 1971-1976.
172. S. Sarkar, S. Niyogi, E. Bekyarova and R. C. Haddon, *Chem. Sci.*, 2011, **2**, 1326-1333.
173. X. Tian, M. L. Moser, A. Pekker, S. Sarkar, J. Ramirez, E. Bekyarova, M. E. Itkis and R. C. Haddon, *Nano Lett.*, 2014, **14**, 3930-3937.

174. M. Chen, W. Li, T. E. da Silveira Venzel, G. Li, M. E. Itkis, R. C. Haddon and E. Bekyarova, *Materials Today*, 2018, **21**, 937-943.
175. M. Chen, W. Li, A. Kumar, G. Li, M. E. Itkis, B. M. Wong and E. Bekyarova, *ACS Applied Materials & Interfaces*, 2019, **11**, 19315-19323.
176. F. Nunzi, F. Mercuri, A. Sgamellotti and N. Re, *J. Phys. Chem. B*, 2002, **106**, 10622-10633.
177. P. Plachinda, D. R. Evans and R. Solanki, *J. Chem. Phys.*, 2011, **135**, 044103.
178. I. Kalinina, E. Bekyarova, S. Sarkar, F. Wang, M. E. Itkis, X. Tian, S. Niyogi, N. Jha and R. C. Haddon, *Macromol. Chem. Phys.*, 2012, **213**, 1001-1019.
179. M. L. Moser, X. Tian, A. Pekker, S. Sarkar, E. Bekyarova, M. E. Itkis and R. C. Haddon, *Dalton Trans.*, 2014, **43**, 7379-7382.
180. M. L. Moser, A. Pekker, X. Tian, E. Bekyarova, M. E. Itkis and R. C. Haddon, *ACS Applied Materials & Interfaces*, 2015, **7**, 28013-28018.
181. A. L. Balch and M. M. Olmstead, *Chem. Rev.*, 1998, **98**, 2123-2166.
182. Y. Matsuo, K. Tahara and E. Nakamura, *J. Am. Chem. Soc.*, 2006, **128**, 7154-7155.
183. M. Sawamura, Y. Kuninobu, M. Toganoh, Y. Matsuo, M. Yamanaka and E. Nakamura, *J. Am. Chem. Soc.*, 2002, **124**, 9354-9355.
184. R. C. Haddon, *J. Comput. Chem.*, 1998, **19**, 139-143.
185. Y. Hashikawa, H. Kawasaki and Y. Murata, *Organometallics*, 2022, **41**, 354-359.
186. H. Werner, *Angew. Chem., Int. Ed.*, 2013, **52**, 6146-6153.
187. K. Motokura, S. Ding, K. Usui and Y. Kong, *ACS Catal.*, 2021, **11**, 11985-12018.
188. F. Zaera, *Coord. Chem. Rev.*, 2021, **448**, 214179.
189. M. Tada and Y. Iwasawa, *Coord. Chem. Rev.*, 2007, **251**, 2702-2716.
190. M. P. Conley, C. Copéret and C. Thieuleux, *ACS Catal.*, 2014, **4**, 1458-1469.